

Portable diagnostic package for Thomson scattering and optical emission spectroscopy on Princeton field-reversed configuration 2 (PFRC 2)

Cite as: Rev. Sci. Instrum. **93**, 113506 (2022); <https://doi.org/10.1063/5.0101849>

Submitted: 03 June 2022 • Accepted: 28 September 2022 • Published Online: 03 November 2022

 N. Kafle,  D. Elliott, B. Berlinger, et al.



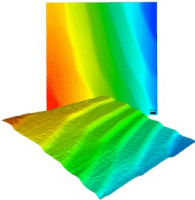
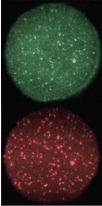
View Online



Export Citation



CrossMark

	<p>Nanopositioning Systems</p> 	<p>Modular Motion Control</p> 	<p>AFM and NSOM Instruments</p> 	<p>Single Molecule Microscopes</p> 
---	--	--	---	--

Portable diagnostic package for Thomson scattering and optical emission spectroscopy on Princeton field-reversed configuration 2 (PFRC 2)

Cite as: *Rev. Sci. Instrum.* **93**, 113506 (2022); doi: [10.1063/5.0101849](https://doi.org/10.1063/5.0101849)

Submitted: 3 June 2022 • Accepted: 28 September 2022 •

Published Online: 3 November 2022



View Online



Export Citation



CrossMark

N. Kafle,¹  D. Elliott¹  B. Berlinger,² Z. He,³  S. Cohen,²  Z. Zhang,³  and T. M. Biewer^{1,a)} 

AFFILIATIONS

¹Oak Ridge National Laboratory, Oak Ridge, Tennessee 37831, USA

²Princeton Plasma Physics Laboratory, Princeton, New Jersey 08543, USA

³University of Tennessee-Knoxville, Knoxville, Tennessee 37996, USA

Note: This paper is part of the Special Topic on Proceedings of the 24th Topical Conference on High-Temperature Plasma Diagnostics.

^{a)}Author to whom correspondence should be addressed: biewerm@ornl.gov

ABSTRACT

An Advanced Research Projects Agency-Energy funded diagnostic system has been deployed to the Princeton field-reversed configuration 2 (PFRC-2) device, located at Princeton Plasma Physics Laboratory. The Portable Diagnostic Package (PDP), designed at Oak Ridge National Laboratory, allows for the measurement of Thomson Scattering (TS) for electron density and temperature and Optical Emission Spectroscopy (OES) for ion temperature, impurity density, and ion velocity. A tunable spectrometer on the PDP with three gratings provides the flexibility to measure low (1 eV) and high (1000 eV) electron temperature ranges from TS. Additionally, using a second spectrometer, the OES diagnostic can survey light emission from various ion excitation levels for wide wavelength ranges. The electron density ($< 2 \times 10^{19} \text{ m}^{-3}$) of plasmas generated in PFRC-2 has been below the PDP TS discrimination threshold, which has made TS signal detection challenging against a high-background of laser stray light. The laser stray light was iteratively reduced by making modifications to the entrance and exit geometry on PFRC-2. Rayleigh scattering experiments on PFRC have yielded the TS discrimination sensitivity to be $> 1 \times 10^{20} \text{ m}^{-3}$ for the PDP. A recently implemented narrow-band notch spectral filter that masks the second harmonic 532 nm Nd:YAG laser wavelength has increased the system's TS light discrimination sensitivity 65 times compared to the instance when the notch filter was not implemented. The hardware implementation including design changes to the flight tubes and Brewster windows will be discussed, along with results from Rayleigh and rotational Raman scattering sensitivity analyses, which were used to establish a quantitative figure of merit on the system performance. The Raman scattering calibration with the notch filter has improved the PDP electron density threshold to $1 \pm 0.5 \times 10^{18} \text{ m}^{-3}$.

Published under an exclusive license by AIP Publishing. <https://doi.org/10.1063/5.0101849>

I. INTRODUCTION

Thomson scattering (TS) as a plasma diagnostic tool was developed in the late 1960s and has been a benchmark diagnostic technique measurement of electron temperature (T_e), electron density (n_e), and, in some cases, the entire electron velocity distribution.^{1–6} The Portable Diagnostic Package (PDP)⁷ has been designed as a traveling diagnostic set consisting of TS along with optical emission

spectroscopy (OES). The PDP is designed to measure T_e , n_e , ion temperature (T_i), and ion density (n_i). The PDP's performance was tested on the Electrothermal-Arc (ET-Arc) source at the Oak Ridge National Laboratory (ORNL) before its deployment.⁸ Helium emission spectra from OES provided the He I line ratios for a collisional radiative model (CRM) and He II emission for the T_i measurement.⁷ Rotational Raman Scattering (RRS) and Rayleigh Scattering (RS) calibrations for TS provided T_e and n_e . After commissioning on the

ET-Arc, the PDP was deployed to the Princeton Field Reverse Configuration 2 (PFRC-2) device located at the Princeton Plasma Physics Laboratory (PPPL).

PFRC 2 is a second generation of the FRC device designed at PPPL. FRC devices are quasi-linear in geometry and have high β ($\beta \equiv$ plasma pressure/magnetic field pressure). High β will allow for the use of aneutronic fuels, such as D-³He rather than conventional D-T fuel.^{9–11} The PFRC-2 vacuum chamber is made out of LEXAN poly-carbonate and has 22.71 cm inner diameter and 83.82 cm axial length. A helicon antenna produces a seed plasma before a rotating magnetic field (RMF) is applied. The helicon plasma can be pulsed or operated at a steady state, but the pulsed RMF nominally produces 4 ms long discharges between 30 and 40 kW power.

Most of the commercial-off-the-shelf (COTS) components of the PDP are modular and portable, which are easy to procure and quick to deliver. The components can also be set up promptly. The PDP largely consists of a Lumibird Q-SMART 1500 (10 Hz, 1500 J at 1064 nm and 850 J at 532 nm) laser, two Teledyne Princeton Instrument Isoplaner SCT320 tunable spectrometers, each with three gratings, two PI-MAX 4-1024f iCCD cameras, Nikon 50 mm f/1.8 lens, 3 × 11 800 μ m fiber optic bundle, and a Gentec pyroelectric energy detector. Using these components (which are modular, have smaller footprint, and are quick to set up) has greatly enabled the PDP's portability. After the commissioning phase, the PDP was set up at PFRC-2 at Princeton Plasma Physics Laboratory (PPPL) within a week, which included loading (at ORNL), transportation, unloading (at PPPL), and reassembly of the system. The Q-SMART 1500 laser and its power supply are physically smaller compared to other TS legacy laser systems. Moreover, with most of the PDP's components in the diagnostic cart,⁷ it can be placed closer to the plasma device without taking significant lab space.

The article organization is as follows: Sec. II will discuss the PDP's integration on PFRC-2, Sec. III A will discuss the RS calibration measurement for threshold electron density estimation without discriminating the central laser wavelength, Sec. III B shows the use of Volume Bragg Grating (VBG) notch filter to reject the stray light, and finally Sec. III C presents the electron density threshold estimation using RRS calibration with the VBG notch filter. Finally, this paper will summarize the findings, provide potential optimization options, and discuss the future work.

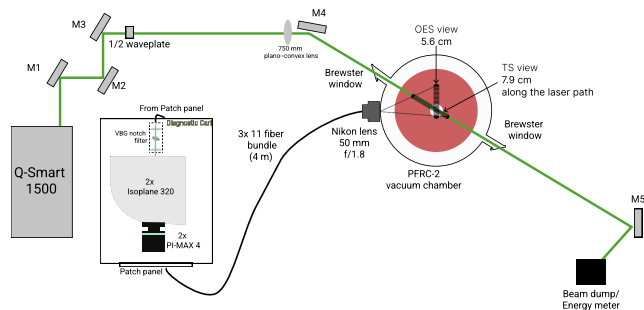


FIG. 1. (not to scale) The schematic of the diagnostic setup. M1–M5 represent 532 nm coated laser graded mirrors. There are two Isoplaner 320 spectrometers and two PI-MAX-4; the local workstation and data storage and acquisition system are located on different shelves of the PDP diagnostic cart.

II. INTEGRATION OF PDP ON PFRC-2

The schematic of the PDP on PFRC-2 is shown in Fig. 1. The 532 nm Nd:YAG is routed upward using 532 nm laser graded coated mirrors from the optical table. The laser enters the vacuum chamber at a 45° angle to the collection optics. The laser traverses across the diameter of PFRC-2. A half wave-plate is placed past mirror 3 (M3) to rotate the laser polarization 90° from vertical to horizontal. Right before steering the beam into the vacuum vessel, a 750 mm plano-convex, focusing lens is used to focus the laser beam at the geometric center of the chamber. Two UV fused silica Brewster-angled windows at the entrance and exit of the laser beam create the air-vacuum interface. After the exit, another mirror directs the laser beam at 90° toward the laser beam dump. The laser energy meter was located within the beam dump. The information from the laser energy measurements is used for both signal and stray light normalization during analysis. The total length of the laser path from the laser to the machine axis is ~2.25 and ~1.95 m from the machine axis to the laser beam dump. The BraggGate VBG notch filter is placed in front of only one spectrometer on the top-shelf.

Of the 33 available optic fibers from the collection bundle, 11 intersect the laser beam path, and the remaining 22 can be used for the OES diagnostics. Eight out of these eleven intersecting views lie above the machine axis, one intersects the machine axis, and the remaining two views lie below the machine axis. The spatial resolution for the TS and OES diagnostics differs because of the 45° angle between the laser path and the collection optics. The total measurement length for TS along the laser path is ~7.9 cm, and the tangency radii for OES span ~5.6 cm for OES, as shown in Fig. 1.

Synchronization of the PDP laser pulses with the PFRC-2 discharges was difficult due to the differences of scale in all the timing. A direct 1 Hz trigger from PFRC-2 to the 10 Hz laser was problematic as it would mean that 90% of the data collected would be stray light and noise. The Q-SMART laser used as part of the PDP has a repetition rate between 9.9 and 10.1 Hz, yet the laser pulse is only 10 ns long. Moreover, the laser must operate for 10–20 min in order to stabilize in energy and it was not possible to trigger PFRC-2 with the laser's internal timing. To ensure optimal laser performance and its synchronization with PFRC-2, a function generator was used to send 10 triggers to the laser at 10.01 Hz. The burst of 10 triggers beginning with every 1 Hz trigger from the PFRC-2 experiment maintained the laser operations in its optimal performance range and kept it synchronized with the PFRC-2 discharge pulse.

Additionally, an “AND circuit” was created so that the intensified camera could be triggered based on the Q-switch of the laser only when the plasma discharge was under way. Figure 2(a) shows the trigger synchronization logic between the TS camera, laser, and PFRC-2 discharge, including the use of the function generator for the laser flash lamp input. This allowed for <50 ns of jitter between the laser timing and the intensified camera timing. Ultimately, this led to an intensified camera integration of 35–75 ns. Ideally, the intensifier on the camera would be perfectly synchronized with the laser and would have its width match that of the laser pulse, so the highest fraction of the collected light would then be from the scattered laser light. Figure 2(b) represents the trigger sequence during plasma discharges.

III. PDP THRESHOLD ELECTRON DENSITY ESTIMATION

A. Threshold from RS in initial PDP configuration

Rayleigh scattering calibration¹² is one of the most common electron density calibration techniques used for TS diagnostics. RS calibration experiments were conducted to identify the electron density discrimination threshold of the PDP for TS measurement on PFRC-2. Since the RS photons are collected close to the laser wavelength, the presence of larger stray light counts influences the instrument's sensitivity calibration. In the initial installation, the entrance and exit apertures on PFRC-2 were ~ 12.4 mm. Assuming the singular Gaussian mode, the beam diameter for the laser was about 9 ± 2 mm, which was roughly the size of the aperture. The Gaussian tail that potentially carried 0.4% of the laser beam might have been interacting with the entrance aperture and scattering into the vessel. A vacuum vent was conducted, where the aperture size was increased to 25 mm ($3 \times$ beam diameter), and an in-vessel view dump was added opposite to the collection optics. With all the above stray light mitigation techniques, the RS calibration measured the n_e discrimination threshold of $>1 \times 10^{20} \text{ m}^{-3}$, which was above the PFRC-2 expected electron density ($<2 \times 10^{19} \text{ m}^{-3}$) for any discernible TS signal from FRC plasmas.

One of the limiting factors in the stray light reduction at PFRC-2 has been the clear vacuum chamber, which allowed the light to exit the vessel from all surfaces and potentially scatter back into the collection optics. A 3D printed mask was custom-made and designed to replace the PI-MAX 4 camera mounting plate. A 1 mm wide mask on the mounting plate at the central pixels would block the laser wavelength. However, the mask did not block the central wavelength as intended. The mask was designed to be normal to the entrance aperture of the camera, but the dispersed light from the spectrometer was likely entering the camera at a non-normal angle. It was empirically estimated to have an offset of $\sim 15^\circ - 20^\circ$ to the left of the detector. Hence, this technique was rejected as a solution.

B. VBG notch filter implementation

Based on the success elsewhere, a narrow-band BraggGate VBG notch filter has been implemented to attenuate the laser stray light intensity.¹ The transmission efficiency of the filter is specified to be at 95%, and the attenuation is specified to be at 99.99%. Two 40 mm focusing lenses are used on either side of the notch filter to collimate the light from the fiber bundle. Figure 3 shows

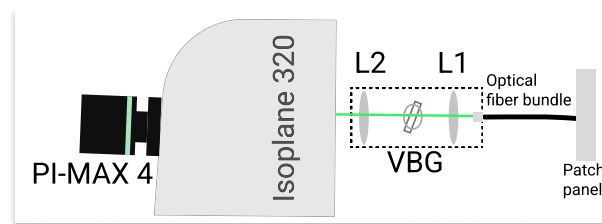


FIG. 3. VBG notch filter setup in front of the spectrometer installed on the top-shelf of the diagnostic cart. L1 and L2 are 40 mm lenses.

the optical layout of the notch filter placed on the top-shelf of the PDP cart.

Figure 4 shows an image of the white-light intensity source on the detector with the notch filter, where alternate fibers (6 out of 11) were illuminated. The VBG notch filter nominally blocks 532 nm wavelength light, which produces the dark band of pixels with reduced intensity. However, the attenuated intensity region is not vertically aligned across the detector but tends to bow inward away from the center fiber channel.

The VBG notch filter blocks light according to a specific physical geometry. Light of a specific wavelength, which is incident on the filter at a specific angle, satisfies the Bragg condition for destructive interference and is not transmitted. In our geometry, imperfectly collimated light originating from fibers that are off-optical-axis encounters the filter at a slight angle; consequently, the Bragg condition is satisfied for light that is at a slightly different wavelength. This manifests itself as a blocking wavelength that is curved in wavelength space for light rays that are increasing with the distance from the optical axis. Consequently, in the current setup, only one out of 11 fiber channels, near the center of the detector, efficiently blocks the 532 nm laser stray light. This reduces the PDP's spatial resolution for the TS measurements from 11 channels to one channel for a single plasma discharge. A single channel TS measurement is still quite significant for the PFRC-2 experiment. A radial profile will be conducted by changing the fibers between plasma discharges.

Figure 5 shows the effectiveness of the spectral notch filter in the stray light attenuation on one fiber channel. Figure 5 (top and bottom, respectively) compares the stray light intensity without the notch filter and with the notch filter in place. Adding the VBG notch filter has reduced the stray light intensity $\sim 65\times$, as

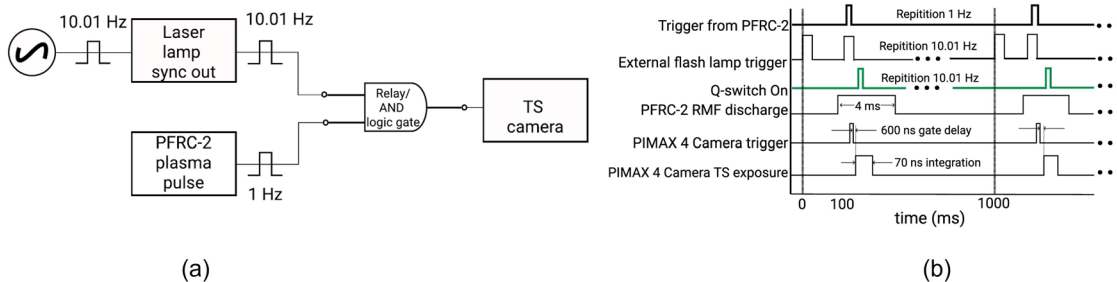


FIG. 2. (a) The synchronization between PDP and PFRC-2 to synchronize the camera trigger and (b) the trigger timing of different components.

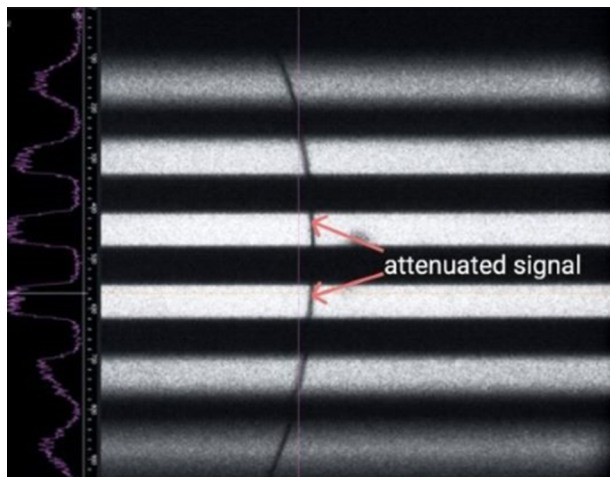


FIG. 4. The image shows six illuminated fiber channels on the detector. The darker bands of narrow pixels in the illuminated channels are the attenuated intensities due to the VBG notch filter.

indicated by the counts in Fig. 5. The attenuation is much less than the vendor specified OD 4 reduction, which gives opportunity for the further improvement of the system. Replacing 40 mm L1 and L2 lenses (shown in Fig. 3) with a longer focal length (~100 mm) lens will improve the collimation, which should reduce the stray light intensity to the vendor specified values.

C. Threshold from RRS in VBG notch filter PDP configuration

The VBG notch filter affects the RS calibration as it blocks the laser wavelength, where the majority of the RS scattered light gets collected. The rotational Raman scattering calibration is another commonly used method to calibrate the density threshold for Thomson scattering.^{1,13,14} RRS spectral peaks represent the transition from one rotational state to another where Stokes (higher energy state) and anti-Stokes (lower energy state) peaks are obtained on the right and the left, respectively, of the excitation wavelength.

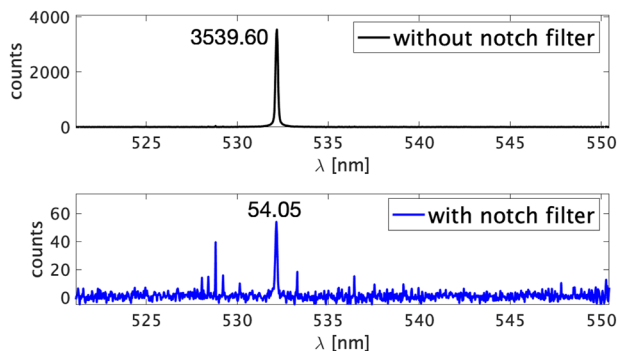


FIG. 5. The top plot shows the straylight intensity without the VBG notch filter, and the bottom plot shows the attenuation from the VBG notch filter on PDP.

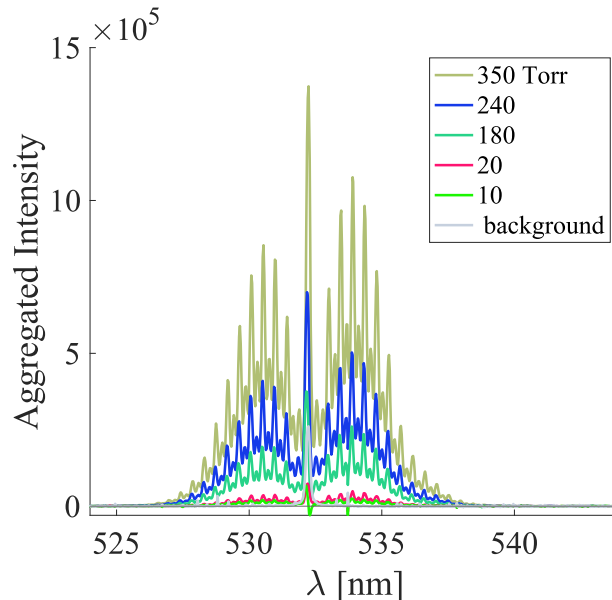


FIG. 6. Rotational Raman scattering signal from nitrogen gas collected at 350, 240, 180, 20, and 10 Torr and at the residual background at 2.4×10^{-6} Torr.

RRS spectra (I_{RRS}) were measured around the 532 nm laser line for nitrogen gas at six different pressure points (350, 240, 180, 20, 10, and 2.4×10^{-6} Torr), as shown in Fig. 6. The gray line is the background signal ($I_{background}$), which is equivalent to the laser stray light near vacuum. The data show the total counts obtained from 6000 laser pulses at an average energy of 440 ± 10 mJ at each N_2 pressure. The plotted data show the RRS signal after subtracting the laser background (i.e., $I_{RRS} = I_{raw_signal} - I_{background}$). The increase in the intensity at the 532 nm wavelength at higher N_2 pressures can be attributed to the RS photons. This is due to the imperfect attenuation by the VBG notch filter at the laser wavelength. Although not shown in Fig. 6, the RRS signal was obtained until 3.3 Torr. Using this pressure, the discrimination n_e threshold for the TS measurement is calculated to be $1 \pm 0.5 \times 10^{18} \text{ m}^{-3}$. The VBG notch filter has improved the PDP's electron density threshold below the estimated electron density in PFERC 2 ($< 2 \times 10^{19} \text{ m}^{-3}$), thus making the TS measurement likely during RMF discharges.

IV. SUMMARY AND FUTURE WORK

This paper presented the deployment and installation of the PDP on PFERC-2. Lessons learned from this project will enable progress in the second iteration of the system. This project encountered several issues associated with high laser stray light, but several solutions have been implemented to improve the PDP's performance. The implementation of the VBG spectral notch filter that blocks the 532 nm light has been the most effective solution in reducing the laser stray light by 65×, hence improving the TS sensitivity threshold of the PDP.

However, the performance of VBG can be further improved by using longer focal length lenses to improve the collimation. The longer image distance may also improve the fiber optics pointing

into the notch filter, which will increase the spatial resolution. Additionally, the effect of a close-packed fiber bundle with a smaller diameter for a signal spatial point can be studied to improve the throughput of the scattered photons. These optimizations should increase the performance of PDP. Since PFRC-2 system upgrade has left the device inoperative for the time being, TS measurements in RMF plasmas may be conducted in the future.

Aside from the TS measurement attempt on PFRC-2, the OES diagnostic has been used to collect the hydrogen line emission (H_{α} , H_{β} , and H_{γ}) spectra. The hydrogen Balmer series can be used to calculate T_e and n_e from the CRM model for hydrogen plasmas. Additionally, Kr II lines collected from the high-resolution OES during the RMF discharge can be used to interpret plasma characteristics. Further analyses of these data are required in the future.

ACKNOWLEDGMENTS

<http://energy.gov/downloads/doe-public-access-plan> This project was supported by the U.S. Department of Energy, Contract No. D.E.-AC05-00OR22725. The authors acknowledge the Program in Plasma Science and Technology for support under DOE Contract No. D.E.-AC02-09CH11466. The authors also greatly appreciate the funding support provided by the Advanced Research Projects Agency-Energy (ARPA-E).

AUTHOR DECLARATIONS

Conflict of Interest

The authors have no conflicts to disclose.

Author Contributions

N. Kafle: Data curation (equal); Formal analysis (equal); Visualization (equal); Writing – original draft (equal); Writing – review & editing (equal). **D. Elliott:** Data curation (equal); Formal analysis (equal); Resources (lead). **B. Berlinger:** Resources (equal). **Z. He:** Data curation (equal); Methodology (equal); Resources (supporting). **S. Cohen:** Investigation (equal); Resources (equal); Supervision (equal); Writing – review & editing (equal). **Z. Zhang:** Conceptualization (equal); Formal analysis (equal); Funding acquisition (equal); Supervision (equal). **T. M. Biewer:** Conceptualization

(equal); Data curation (equal); Formal analysis (equal); Funding acquisition (equal); Methodology (equal); Resources (equal); Supervision (equal); Writing – review & editing (equal).

DATA AVAILABILITY

The data that support the findings of this study are available from the corresponding author upon reasonable request.

REFERENCES

- ¹B. Vincent *et al.*, “A compact new incoherent Thomson scattering diagnostic for low-temperature plasma studies,” *Plasma Sources Sci. Technol.* **27**, 055002 (2018).
- ²B. L. Klarenaar *et al.*, “How dielectric, metallic and liquid targets influence the evolution of electron properties in a pulsed He jet measured by Thomson and Raman scattering,” *Plasma Sources Sci. Technol.* **27**, 085004 (2018).
- ³T. N. Carlstrom *et al.*, “Thomson scattering measurements on DIII-D using in-vessel laser mirrors and lenses to diagnose a new divertor location,” *Rev. Sci. Instrum.* **89**, 10C111 (2018).
- ⁴P. Shi *et al.*, “Incoherent Thomson scattering system for PHASE space MAPPING (PHASMA) experiment,” *Rev. Sci. Instrum.* **92**, 033102 (2021).
- ⁵B. Vincent, S. Tsikata, and S. Mazouffre, “Incoherent Thomson scattering measurements of electron properties in a conventional and magnetically-shielded Hall thruster,” *Plasma Sources Sci. Technol.* **29**, 035015 (2020).
- ⁶H. Tojo *et al.*, “Design of JT-60SA core Thomson scattering diagnostic system,” *Rev. Sci. Instrum.* **92**, 043556 (2021).
- ⁷N. Kafle *et al.*, “Design and implementation of a portable diagnostic system for Thomson scattering and optical emission spectroscopy measurements,” *Rev. Sci. Instrum.* **92**, 063002 (2021).
- ⁸Z. He *et al.*, “Multi-channel Thomson scattering measurements on an electrothermal arc source,” *Rev. Sci. Instrum.* (Submitted) (2022).
- ⁹S. Cohen *et al.*, “RF plasma heating in the PFRC-2 device: Motivation, goals and methods,” *AIP Conf. Proc.* **1406**, 273–276 (2011).
- ¹⁰S. A. Cohen and A. H. Glasser, “Ion heating in the field-reversed configuration by rotating magnetic fields near the ion-cyclotron resonance,” *Phys. Rev. Lett.* **85**, 5114–5117 (2000).
- ¹¹S. A. Cohen *et al.*, “Formation of collisionless high- β plasmas by odd-parity rotating magnetic fields,” *Phys. Rev. Lett.* **98**, 145002 (2007).
- ¹²K. Warner and G. M. Hieftje, “Thomson scattering from analytical plasmas,” *Spectrochim. Acta, Part B* **57**, 201–241 (2002).
- ¹³J. Barrett, “Generation of coherent anti-Stokes rotational Raman radiation in hydrogen gas,” *Appl. Phys. Lett.* **29**, 722–724 (1976).
- ¹⁴B. P. LeBlanc, “Thomson scattering density calibration by Rayleigh and rotational Raman scattering on NSTX,” *Rev. Sci. Instrum.* **79**, 10E737 (2008).